



HAL
open science

Imidazole Functionalized Graphene and Carbon Nanotubes for CO₂ detection

Mohamed Bensifia, Fatima Bouanis, Céline Léonard

► **To cite this version:**

Mohamed Bensifia, Fatima Bouanis, Céline Léonard. Imidazole Functionalized Graphene and Carbon Nanotubes for CO₂ detection. *Journal of Molecular Structure*, 2022, 1259, pp.132719. 10.1016/j.molstruc.2022.132719 . hal-03605420

HAL Id: hal-03605420

<https://hal.science/hal-03605420v1>

Submitted on 22 Jul 2024

HAL is a multi-disciplinary open access archive for the deposit and dissemination of scientific research documents, whether they are published or not. The documents may come from teaching and research institutions in France or abroad, or from public or private research centers.

L'archive ouverte pluridisciplinaire **HAL**, est destinée au dépôt et à la diffusion de documents scientifiques de niveau recherche, publiés ou non, émanant des établissements d'enseignement et de recherche français ou étrangers, des laboratoires publics ou privés.



Distributed under a Creative Commons Attribution - NonCommercial 4.0 International License

Imidazole Functionalized Graphene and Carbon Nanotubes for CO₂ detection

Mohamed BENSIFIA^a, Fatima BOUANIS^{b,c}, and Céline LEONARD^{a,*}

- a) Univ Gustave Eiffel, Univ Paris Est Creteil, CNRS, UMR 8208, MSME, F-77454 Marne-la-Vallée, France
- b) Univ Gustave Eiffel, COSYS-LISIS, F-77454 Marne-la-Vallée, France
- c) Laboratoire de Physique des Interfaces et des Couches Minces (LPICM), CNRS, Ecole Polytechnique, Institut Polytechnique de Paris, 91128 Palaiseau, France

*corresponding author. Tel.: +33.1.60.95.73.18

E-mail address: celine.leonard@univ-eiffel.fr (Céline LEONARD)

Mohamed.bensifia@univ-eiffel.fr (Mohamed BENSIFIA)

Key words: SWNT, graphene, imidazole, CO₂, gas detection, DFT

Abstract

The effect of the non-covalent functionalization of single-walled carbon nanotubes (SWNTs) and graphene with imidazole is evaluated using Density Functional Theory (DFT) with the aim of improving the CO₂ detection. Both metallic and semi-conducting SWNTs are investigated. The interaction of imidazole ring with different carbon nanomaterials is analysed, as well as the adsorption of CO₂ before and after the surface functionalization process. The binding energies, the energy bandgaps, the Fermi levels, and the charge transfer process have been computed for all the possible fragments and for the total interacting systems. The functionalization of SWNT(8,0) and graphene by an imidazole ring increases the stability of CO₂ physisorption and improves the positive charge transfer from CO₂ to the carbon material, confirming that such functionalization can be a viable strategy for CO₂ detection.

1. Introduction

The detection of air pollutants and toxic gases such as carbon monoxide (CO), nitrogen oxide (NO), ammonia (NH₃), carbon dioxide (CO₂), and sulfur dioxide (SO₂) is a very important challenge to be solved¹. CO₂ is a colorless and odorless gas, used in a wide range of applications including pharmaceutical, agricultural, cosmetics and food industries². It is among the most dangerous and prevalent greenhouse gases emitted. Moreover, extended exposure to high CO₂ concentrations can cause serious risks to human life eventually resulting in unconsciousness and death due to suffocation. Several alternative sensors have been investigated to detect CO₂ such as optical sensors^{3, 4}, electrochemical sensors⁵, and polymer-based sensors⁶. All these systems show a high sensitivity to CO₂ down to the low concentrations. However, each has its drawbacks and limitations, with the most common being excessive price and high power-consumption, and, sometimes, high operating temperature. Frequently those sensors are complex and bulky⁷. Consequently, development of a new generation of highly sensitive and selective gas sensors to detect CO₂ at room temperature is required. Furthermore, there is a growing need to develop accurate and reliable sensors that can operate in wide ranges of temperatures and pressures.

Recently, carbon based nanomaterials such as graphene and carbon nanotubes (CNTs), attracted significant interest, due to their unique physical, chemical and mechanical properties^{8, 9, 10, 11}. These properties make them promising candidates for a wide range of applications in science and engineering^{12, 13}. The most common one is environmental sensing due to their large surface-to-volume ratio as well as high electrical conductivities and a low electrical noise¹⁴. Carbon nanomaterials have been found to be sensitive towards different gas molecules^{15, 16}. However, these materials show weak responses and low selectivity toward specific gas molecules due to the weak interaction between them and specific molecules. Various strategies have been studied to enhance the sensitivity and selectivity of sensors based on carbon nanomaterials to specific gases. One such strategy is functionalization by chosen chemical species.

Surface functionalization of the sensor-based nanomaterials is often used to improve the selectivity and sensitivity towards the targeted gas¹⁷. The chemical sensing mechanism is related to the question of how gas/molecular species interact with the functionalized nanomaterials and how this interaction affects their electrical properties. Therefore, the choice of the chemical entities used for the functionalization is critical, because the newly added chemical functionality

should not only provide additional properties to be used in sensing, but it also should not disturb the intrinsic electrical properties of carbon nanomaterials.

The chemical functionalization can be carried out by non-covalent and covalent approaches^{18, 19, 20, 21, 22, 23}. The latter involves a chemical link between the nanomaterial and a specific functional group that guarantees strong and stable interactions. However, it destroys the extended π -system of nanomaterials, which adversely affects their electrical properties. An efficient strategy is to design hybrids between nanomaterials and the chemical modules through non-covalent assembly, often through π - π interactions^{24, 25}. In such a case, the intrinsic charge transport properties are unaffected or only slightly affected. The non-covalent functionalization of carbon nanomaterials has been demonstrated with different kinds of functionalization groups, either organic or inorganic, such as polymers²⁶, metallic nanoparticles²⁷, porphyrins^{28, 29}, phthalocyanines³⁰ and enzymes³¹.

Among the most exciting candidate molecules are imidazole and its derivatives that occupy a unique place in the field of CO₂ capture and storage³². The N-heterocyclic compound presents a peculiar structure with a small conjugated ring. Furthermore, imidazole derivatives can combine with different receptor systems through diverse weak interactions due to the presence of an electron-rich feature in its structure. These molecules have been investigated as promising agents in various applications, among them electrochemical sensors³³, gas sensors³⁴ and catalysis³⁵.

N. Garg et al.³⁴ reported the sensitivity of a composite of the zeolite imidazole framework and reduced graphene oxide towards NH₃. They showed that developed sensor is sensitive and selective to NH₃ gas. Furthermore, they demonstrated that these devices are reproducible and offer a stable response against humidity and some other volatile compounds. Li et al.³⁶ produced single-walled carbon nanotubes (SWNTs) chemoresistive sensors functionalized with imidazolium-based ionic liquids. They demonstrated that the functionalized SWNTs sensors exhibit a very low detection limit toward CO₂ down to 50 ppm at room temperature compared to that of pristine SWNTs sensors. They also investigated the selectivity of response to different gases and showed that the sensor is highly selective and resistant to the interference of relative humidity.

The present paper is devoted to the study the effects of the non-covalent functionalization of carbon nanomaterials by imidazole in a view to improve the detection of CO₂ by carbon nanomaterial-based sensors. This detection is based on the variation of the electronic properties of the material. Two types of SWNTs (metallic and semi-conducting) and graphene have been compared to evaluate their respective performances. Periodic ab initio calculation is the perfect tool to determine the change of the electronic properties of extended periodic nanomaterials such as graphene or carbon nanotubes with respect to functionalization and to gas capture. The use of Bloch functions expanded as linear combinations of atom-centered Gaussian functions allows one to correctly describe all the electrons of the system: both those of the material and the molecules.

2. Computational Methods

Restricted periodic Density Functional Theory (DFT) calculations (closed shell) were applied using the CRYSTAL17 code³⁷, in order to obtain the optimal geometries and electronic properties of graphene/SWNTs, graphene-imidazole/SWNTs-imidazole, and graphene-imidazole-CO₂/SWNTs-imidazole-CO₂, respectively. An advantage of CRYSTAL17 is the treatment of 2D slabs without considering the periodicity perpendicular to the surface. Graphene was modelled as 5 × 6 supercell (60 atoms), SWNT(8,0), SWNT(5,5) with supercells of 3 × 3, 6 × 6 (96 and 120 atoms), respectively. The PBE0 functional³⁸ has proved to be well adapted for describing semiconductor extended systems³⁹ and PBE⁴⁰ is suitable for graphene^{41, 42, 43}. PBE0 and PBE calculations have been performed for the SWNT(8,0) and SWNT(5,5) systems, respectively. Furthermore, in order to better compare the graphene and SWNTs results, the graphene was modelled using both PBE and PBE0. These functionals have the advantage of being non-empirical and parameter free. The carbon, nitrogen, hydrogen and oxygen atoms of all systems have been described by the all electron pob-TZVP basic set⁴⁴. For all the geometrical optimizations, the long-range van der Waals interactions were taken into account with D3 semi-empirical correction by Grimme combined with Becke-Johnson damping D3(BJ)⁴⁵. This correction improves the long-range electron correlation of DFT functionals, essential in the description of the long-range interaction between all fragments of this work. It has been checked that this basis set associated to PBE0-D3 and PBE-D3 allows to correctly reproduce imidazole, CO₂, imidazole-CO₂ structures and their interactions. In this paper, the Fermi levels for these

molecular systems are determined as the highest occupied molecular orbital (HOMO) energy levels.

The selection of the \vec{k} sampling is essential in order to have a good description of graphene and SWNTs⁴⁶. 6, 7 and 74 \vec{k} vectors have therefore been employed to model the free SWNT(8,0), SWNT(5,5), and graphene, respectively. For the geometry optimizations and the evaluation of the Fermi energies, the 12×12 Monkhorst-Pack/Gilat grid of k-points was applied to represent the Brillouin zone for graphene and SWNT(5,5), and the 10×10 grid for SWNT(8,0) including 2D systems. For state densities (DOS) and band structures, denser grids of 50×50 and 12×12 were used for SWNTs and graphene, respectively. The band structure for graphene system is described on the reciprocal path of the Brillouin zone Γ -M-K- Γ where $\Gamma = (0, 0, 0)$, M = $(\frac{1}{2}, 0, 0)$, K = $(\frac{1}{3}, \frac{1}{3}, 0)$, and for SWNTs systems on Γ -K where K = $\frac{\pi}{a}$, and a is the lattice parameter.

The Self-Consistent Field (SCF) energy convergence of SWNT(8,0) systems was achieved using LEVSHIFT 10 1. The truncations of the coulomb and exchange terms were controlled by five thresholds: 11,11,11,15 and 30. For SWNT(5,5), the default value of the truncation tolerances was used (see CRYSTAL manual in Ref.⁴⁷ for exact details). For systems that include graphene, the SCF energy convergence is achieved using Anderson quadratic mixing. The Fermi surface is smeared with a Gaussian of 0.005 Hartree for graphene and SWNT(5,5) systems. In all our calculations FMIXING 20 has been used and the SCF energy threshold values have been set to 10^{-7} (default value), 10^{-9} , and 10^{-9} Hartree for SWNT(8,0), SWNT(5,5), and graphene, respectively. The net charge transfer (Δq) was calculated using the Mulliken population analysis⁴⁸.

The binding energy was calculated for each interacting structure taking into account the basis set superposition error (BSSE) using counterpoise (CP) corrections^{49, 50} and the geometrical distortion:

$$E_b = E_{AB}^{ab} - (E_A^a + E_B^b) - (E_{A^*}^{ab} + E_{B^*}^{ab}) + (E_{A^*}^a + E_{B^*}^b) \quad (1)$$

where E_{AB}^{ab} is the energy of the AB complex at its equilibrium geometry using the total complex basis set, ab ; E_A^a is the energy of the isolated A fragment at its equilibrium geometry (idem for B)

using the fragment basis set, a . $E_{A^*}^{ab}$ is the energy of the A fragment at the equilibrium geometry in the AB complex using the total complex basis set, ab with B "ghost" massless atom (idem for B); $E_{A^*}^a$ is the energy of the A fragment at the equilibrium geometry in the AB complex (idem for B) using the fragment basis set, a .

The total density of states (DOS) of all the systems have been computed using PBE and/or PBE0 functionals. In order to highlight the contribution of each constituent of the complexes, the molecular orbitals of the molecular fragments (imidazole and CO_2) have also been computed at the equilibrium geometries using GAUSSIAN code ⁵¹. The same computational methods and basis set have been employed, i.e. PBE0-D3BJ/pob-TZVP and PBE-D3BJ/pob-TZVP. The Multiwfn software ⁵² was used, with adjustment of the scale ratio for the DOS curve at 130/200 eV and a gaussian broadening with full width at half maximum (FWHM) at 0.100 eV.

3. Results and Discussions

3.1 Carbon nanomaterials

As the first step, structural parameters such as bond lengths of graphene, SWNT(5,5), and SWNT(8,0) were investigated using the DFT methods. Figure 1 shows the zigzag SWNT(8,0) and armchair SWNT(5,5) geometric structures. Two different types of bonds are identified in SWNTs: the $d_{\text{C-C}(a)}$ nanotube axis and the $d_{\text{C-C}(c)}$ nanotube circumference. The fully optimized structural parameters are reported in Table 1.

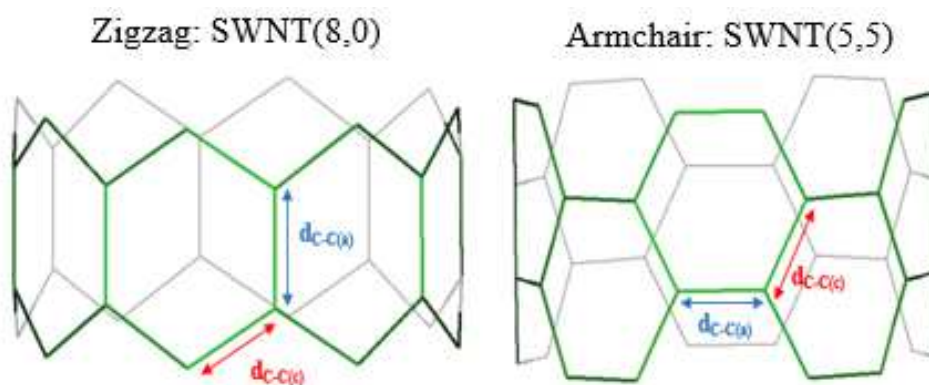


Figure 1: Geometries of the zigzag SWNT(8,0) nanotube and of the armchair SWNT(5,5) nanotube with two types of bonds: the $d_{\text{C-C}(a)}$ nanotube axis and the $d_{\text{C-C}(c)}$ nanotube circumference.

Table 1 summarizes the comparison between experimental values, previous works and optimized parameters of zigzag (8,0), armchair (5,5) SWNTs, and graphene, i.e. the C-C bond length (\AA), the lattice parameter a (\AA), the diameter d_t (\AA), and the band gap E_g (eV). According to the results presented in Table 1, the d_{C-C} bonds are elongated in SWNTs compared to the graphene. For the graphene, the d_{C-C} length computed by the PBE-D3/pob-TZVP method is the closest to the experimental value.

The armchair SWNT(5,5) and graphene present a zero energy bandgap ($E_g = 0$ eV), unlike the zigzag SWNT(8,0). The PBE0 functional has been shown to provide the most accurate value of the band gap for SWNT(8,0), compared to the experimental value. This functional combines PBE generalized gradient functional and Hartree-Fock (HF)⁵³ exchange with predefined coefficients³⁸. It has been shown previously that the inclusion of the exact HF exchange compensates the error of fractional electron occupations⁵⁴. For SWNT(8,0), the PBE and PBE0 lead to different results, especially for the values of the energy bandgaps as expected from previous studies^{55, 56, 57, 58}. However, the PBE0 functional gives $E_g = 1.570$ eV using the pob-TZVP basis set, similar to the experimental value of 1.598 eV^{59, 60}. Both functionals give a SWNT(8,0) diameter in agreement with the experimental value⁵⁹.

Table 1: Comparison of the parameters of graphene and zigzag (8,0), armchair (5,5) SWNTs: C-C bond length (d_{C-C} of graphene, and $d_{C-C(a)}$ the nanotube axis, $d_{C-C(c)}$ the nanotube circumference of SWNTs (\AA)), diameter d_t (\AA), lattice parameter a (\AA), band gap (eV).

System	Methods	Bond length d_{C-C} (\AA)		d_t (\AA)	a (\AA)	E_g (eV)
		$d_{C-C(a)}$	$d_{C-C(c)}$			
Graphene	PBE-D3/pob-TZVP	1.420		∞	2.460	0
	PBE0-D3/pob-TZVP	1.411			2.444	0
	Exp ⁶¹	1.420			2.459	0
SWNT(5,5)	PBE-D3/pob-TZVP	1.423	1.424	6.849	2.459	0.000
	PBE0-D3/pob-TZVP	1.414	1.414	6.810	2.443	0.000
	B3LYP/6-1111G(d) ⁶²	1.423	1.432	6.877	2.458	-
	PW91 ⁶³	1.423	1.427	6.780	2.456	0.000
	B3LYP ⁵⁸			5.570	2.470	0.000
SWNT(8,0)	PBE-D3/pob-TZVP	1.414	1.430	6.351	4.256	0.583
	PBE0-D3/pob-TZVP	1.404	1.421	6.310	4.227	1.570
	B3LYP ⁵⁸			6.410	4.260	1.283

	B3PW/6-1111G(d) ⁶²			6.350		1.304
	PBE ⁶²					0.566
	PW91 ⁶³	1.412	1.433	6.260	4.248	1.200
	LDA(GW) ⁶⁴					0.5 (1.80)
	GW ⁶⁵					1.750
	COHSEX ⁶⁶					1.780
	Katura's diagram ⁶⁷					1.990
	Exp ^{59 60}			6.340		1.598

3.2 Imidazole-CO₂

For a better understanding of the interaction of CO₂ molecules with imidazole, a complete study of all the possible interactions between both molecules has been made following Ref.⁶⁸. This step allows us to verify that the CRYSTAL code calculations well reproduce DFT results obtained with a non-periodic code. Three equilibrium structures have been found, denoted in this paper Im-CO₂ I, Im-CO₂ II, and Im-CO₂ III. Two structures result from a π -type stacking interaction: the first one, denoted Im-CO₂ I (see Figure 2), corresponds to an in-plane global geometry of the imidazole-CO₂ complex, with the CO₂ carbon atom in front of the H-free nitrogen atom of imidazole. The second one is denoted Im-CO₂ II (see Figure 2) and is an out-of-plane organization in which the CO₂ carbon atom is located above the C-C bond of the imidazole cycle. The third structure, Im-CO₂ III (see Figure 2), presents an interaction between one of the CO₂ oxygen atoms and the hydrogen atom of the imidazole amino group, forming a σ -type hydrogen bond. The binding energies for these three geometries were calculated and compared with previously published results (see Table 2). Data presented in Table 2 indicate that PBE0-D3/pob-TZVP and PBE-D3/pob-TZVP values are similar. The inclusion of the Grimme's dispersion term is very important for an accurate description of the imidazole and CO₂ interaction and our results are within the same order of magnitude as the previously calculated values^{68, 69}. To the best of our knowledge, there is no experimental data available for the imidazole-CO₂ system. The most stable geometry is Im-CO₂ I, with $E_b = 20.58$ kJ/mol and a minimum distance of $d_m = 2.68$ Å between the fragments with the PBE0-D3/pob-TZVP method, favored by a weak electron donor-acceptor mechanism from imidazole towards CO₂ through the interaction between the carbon atom of CO₂ and the nitrogen atom of the heterocycle. The Im-CO₂ II structure is more stable than the Im-CO₂ III one.

Table 2: Comparison of binding energies, E_b (kJ/mol), using Equation (1), and minimal distance, d_m (Å), calculated at PBE0-D3/pob-TZVP and *PBE-D3/pob-TZVP levels of theory and compared with previous works^{68,69}. The geometrical structures are shown in Figure 2.

System	E_b (kJ/mol) Present work	E_b^a (kJ/mol) Previous works	d_m (Å) Present work	d_m^b (Å) Previous works
Imidazole-CO ₂ (Im-CO ₂ I)	-20.58	-20.23	2.68	2.78
Imidazole-CO ₂ (Im-CO ₂ I)*	-19.65		2.66	
Imidazole-CO ₂ (Im-CO ₂ II)	-10.45	-14.36	3.00	3.09
Imidazole-CO ₂ (Im-CO ₂ II)*	-10.49	-11.10 ^c	2.99	
Imidazole-CO ₂ (Im-CO ₂ III)	-9.33	-9.65	2.16	2.13
Imidazole-CO ₂ (Im-CO ₂ III)*	-9.16	-9.30 ^c	2.16	2.26 ^c

^aCCSD(T)-F12/VTZF12+ BSSE⁶⁸, ^bMP2/aug-cc-pVTZ⁶⁸, ^cPBE-D3/aug-cc-pVTZ⁶⁹

3.1 CO₂-imidazole interacting with carbon nanomaterials

The geometries of all systems have been fully optimized. First, the possible interactions of CO₂ with surfaces of the carbon nanomaterials, before functionalization, have been studied. For the CO₂ adsorption on graphene and SWNTs surfaces, the most stable structures are of π stacking type and are labeled as graphene-CO₂ (G-I), SWNT(5,5)-CO₂ (55-I), and SWNT(8,0)-CO₂ (80-I) in Figure 2. To improve the selectivity of SWNTs and graphene to the CO₂ detection, non-covalent functionalization of the carbon nanomaterials with the imidazole molecule have been performed. In all optimized structures, the imidazole is parallel to graphene and SWNTs surfaces due to π -stacking interactions. Next, the adsorptions of the CO₂ molecule in functionalized SWNTs and functionalized graphene have then been studied. In order to obtain the most stable structure of adsorbed CO₂ on the functionalized graphene (graphene-imidazole G-II complex), various types of initial adsorption geometries have been considered. Three optimized organizations of CO₂-imidazole on the surface of graphene have been identified, corresponding to the three possible interacting structures between imidazole and CO₂ fragments discussed in the previous subsection. They are labeled in this paper as G-III, G-IV, and G-V, respectively. Unlike graphene, only one structure is possible for each type of SWNTs between the SWNT-imidazole complex and CO₂. The interaction of imidazole with the SWNTs surface depends on the SWNT structure (zigzag or armchair). The interactions between SWNTs-imidazole (SWNT(5,5)-imidazole 55-II and SWNT(8,0)-imidazole 80-II complexes) with CO₂ molecule are of π -type, with a stacking structure for SWNT(5,5)-imidazole 55-III and an in-imidazole-plane one for SWNT(8,0)-imidazole 80-III, respectively (see Figure 2).

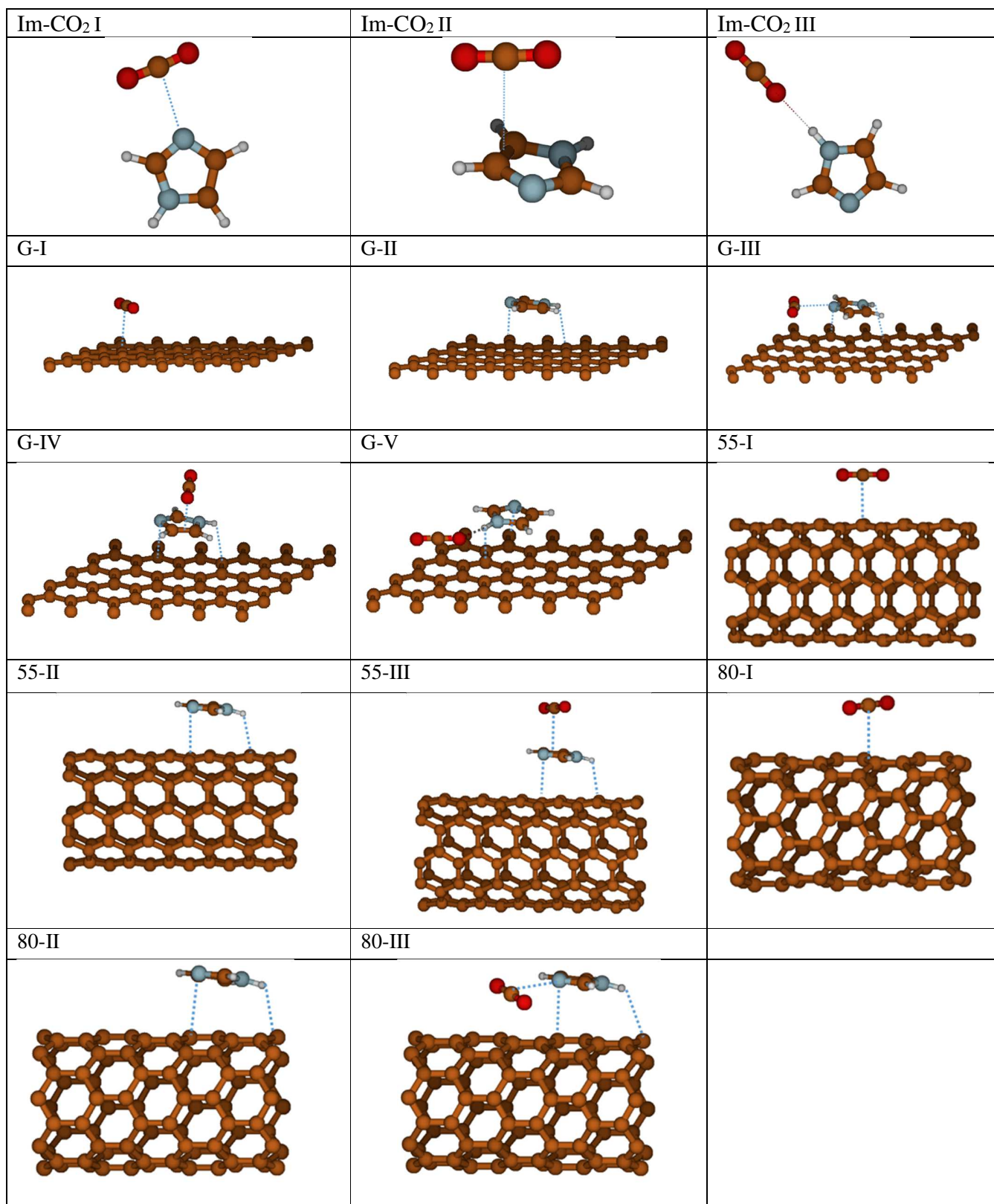


Figure 2: Optimized geometries and minimal distances between the fragments at the PBE0-D3/ pob-TZVP and PBE-D3/pob-TZVP (for SWNT(5,5) including systems only) levels of theory.

The binding energies (E_b in kJ/mol) and minimal distances (d_m in Å) for all systems have been computed and given in Table 3. For graphene, the PBE and PBE0 values are very close. The interactions of CO₂ and imidazole molecules with the surface of graphene are slightly more stable than with the SWNTs surfaces. The present results are in agreement with LDA for SWNT(5,5)-CO₂, and with PW91 and rev-vdW-DF2 for graphene-CO₂, in agreement with the fact that PBE-D3 and vdW-DF2 give accurate equilibrium distances and binding energies for rare gas atoms interacting with graphene⁷⁰. Experimentally determined binding energy is only available for CO₂ on graphene/SiC(0001), and is about 10 kJ.mol⁻¹ larger than our values. This discrepancy could be due to the presence of SiC(0001) substrate that could bring some additional interactions with CO₂. For all carbon materials, imidazole is more strongly adsorbed than CO₂. The minimal distances for the CO₂ adsorption on the different surfaces are around 3 Å, whereas this distance is about 2.7 Å for the imidazole adsorption.

For G-III and 80-III systems, the distance between CO₂ and imidazole is larger than in the corresponding isolated imidazole-CO₂ systems. In these structures, both CO₂ and imidazole interact with the surface of graphene/SWNT(8,0) (see Figure 2). For G-IV, G-V, and 55-III, the distances are slightly shorter than in imidazole-CO₂ (Im-CO₂ II and Im-CO₂ III).

The binding energy of CO₂ to functionalized graphene or SWNT(8,0) is larger than to corresponding pristine carbon nanomaterials. In both systems, the most stable organization, G-III or 80-III, corresponds to an optimized geometry where CO₂ is located with respect to imidazole as in Im-CO₂ I, the most stable Im-CO₂ conformation ($E_b = -20.58$ kJ/mol, see Table 2). G-IV and 55-III correspond to global π -stacking organizations with no increase of the binding energy of CO₂ after functionalization. In structure G-V, imidazole and CO₂ form a σ -type hydrogen bond on the surface of graphene. This structure corresponds to the strongest binding of the imidazole-CO₂ complex with all the carbon materials studied in the present work, $E_b = -34.71$ kJ/mol. The interaction between isolated imidazole and CO₂ in Im-CO₂ III has the lowest binding energy ($E_b = -9.33$ kJ/mol), such that both CO₂ and imidazole can interact more with the graphene surface than between each other (see Tables 2 and 3). For this geometrical arrangement, the binding of the gas molecule is only slightly increased by the functionalization.

Table 3: Comparison of binding energies, E_b (kJ/mol), using Equation (1), and minimal distance, d_m (Å), calculated at the PBE0-D3/pob-TZVP (for SWNT(8,0) and graphene including systems) and *PBE-D3/pob-TZVP (for SWNT(5,5) and graphene including systems) levels of theory. The geometrical structures are shown in Figure 2.

System A-B or A-B-C	E_b (kJ/mol) A+B or (A+B)+C	E_b (kJ/mol) A+(B+C)	d_m (Å) A+B	d_m (Å) B+C
Graphene-CO ₂ (G-I)	-14.38		3.02	
Graphene-CO ₂ (G-I)*	-14.08		3.02	
PW91 ⁷¹	-13.12			
rev-vdW-DF2 ⁷²	-15.9			
vdW-DF1 ⁷²	-24.3		3.4	
optB86b-vdW ⁷²	-24.7		3.2	
Exp (graphene/SiC(0001)) ⁷²	-26.4 ± 1.5			
Graphene-imidazole (G-II)	-19.78		2.77	
Graphene-imidazole (G-II)*	-19.14		2.73	
Graphene-imidazole-CO ₂ (G-III)	-31.38	-30.13	2.88	2.76
Graphene-imidazole-CO ₂ (G-III)*	-29.95	-27.97	2.84	2.73
Graphene-imidazole-CO ₂ (G-IV)	-11.98	-22.15	2.79	2.98
Graphene-imidazole-CO ₂ (G-IV)*	-11.80	-20.77	2.76	2.96
Graphene-imidazole-CO ₂ (G-V)	-20.15	-34.71	3.07	2.10
Graphene-imidazole-CO ₂ (G-V)*	-19.21	-35.84	3.06	2.10
SWNT(5,5)-CO ₂ (55-I)*	-11.75		2.99	
LDA ⁷³	-10.52			
SWNT(5,5)-imidazole (55-II)*	-14.50		2.74	
SWNT(5,5)-imidazole-CO ₂ (55-III)*	-11.07	-15.41	2.75	2.97
SWNT(8,0)-CO ₂ (80-I)	-11.43		2.95	
SWNT(8,0)-imidazole (80-II)	-15.57		2.63	
SWNT(8,0)-imidazole-CO ₂ (80-III)	-26.85	-19.93	2.81	2.87

* PBE-D3/pob-TZVP

The graphene displays a semi-metallic character with a linear dispersion of valence and conducting bands at the Fermi level, SWNT(8,0) also displays semi-conducting properties, whereas SWNT(5,5) has a metallic character. To investigate the changes in the electronic structures of graphene and SWNTs caused by the adsorption of molecules on their surfaces, Fermi levels (E_f in eV) and energy bandgaps (E_g in eV) have been computed and reported in Table 4. The charge transfers (Δq) between fragments have also been determined using a Mulliken analysis and the values are given in Table 5. The physisorption should impact the electronic levels of both the material surfaces and the adsorbate⁷⁴. The adsorption of the molecules on the surface of graphene and SWNT(5,5) does not open up the gap between the valence band and the conduction band, indicating that the molecule adsorptions induce only weak perturbations on the electronic structures of the carbon nanomaterials. For semi-conductor

SWNT(8,0), E_g increases only by 0.0012 eV with the CO₂ adsorption and decreases by 0.0097 eV with the functionalization of SWNT(8,0) by imidazole. The weak variations of the bandgap result from the high HOMO-LUMO energy differences in the molecules, i.e. 11.7521 eV and 7.7999 eV for the equilibrium geometries of CO₂ and imidazole, respectively. The more significant HOMO-LUMO difference of CO₂ involves a weaker bandgap variation of the global CO₂-adsorbed system.

According to the variations of the bandgaps, of the Fermi levels, and the charge transfers of the different systems, i.e. graphene/SWNTs, graphene/CO₂, graphene/SWNTs-imidazole, graphene/SWNTs-imidazole-CO₂, the effect of the adsorption of molecules on the electronic structures of the material is confirmed to be weak. However, variations have been analyzed. The Fermi levels are systematically downshifted after each molecule adsorption onto the graphene or SWNTs surfaces, as can be seen in Table 4. The variation of the Fermi levels has also been plotted in Figure 3 to show the variation of the Fermi levels upon the adsorption of CO₂, imidazole and imidazole-CO₂ complex onto the graphene/SWNTs surfaces. The downshift is more important in graphene systems than in SWNTs ones. It results in electron transfer from the carbon nanomaterials towards the adsorbed molecules (see Table 5). When the Fermi level decreases upon the molecule adsorption onto the graphene surface, the graphene gives electrons to adsorbates. The graphene is p-doped and the molecule is electron acceptor. The result obtained for CO₂ is in agreement with previous work⁷⁵.

The difference in the Fermi level variations for three graphene-imidazole-CO₂ systems can be understood using the analysis of the imidazole-CO₂ HOMO variations with geometrical arrangements. In Im-CO₂, the HOMO orbitals are mainly composed of imidazole-free HOMO ones. In Im-CO₂ I and Im-CO₂ II, the HOMO energies decrease with respect to the free imidazole HOMO energy (see Table 4), indicating that the adsorption of CO₂ involves an electron transfer from imidazole towards CO₂. This is also confirmed by the charge values for the corresponding systems, given in Table 5. The charge transfer increases with the decrease of the HOMO energy level. It can also be noticed that the charge transfer is more efficient in the π - π stacking bonding type between imidazole and CO₂ in Im-CO₂ II. In Im-CO₂ III, the situation is reversed. CO₂ is electron donor to imidazole and the electron transfer is weaker due to the particularity of the hydrogen bond-type interaction. This results in a weaker upshift of the HOMO energy of 0.1613

eV and a net charge of 0.0046e in CO₂. The Fermi level variations in the G-III, G-IV, and G-V graphene-imidazole-CO₂ systems follow the same trends as in G-II graphene-imidazole system.

Table 4: Fermi levels, E_f (eV), and bandgap energies, E_g (eV) at the PBE0-D3/pob-TZVP and *PBE-D3/pob-TZVP levels of theory. The geometrical structures are shown in Figure 2. For molecules, the Fermi levels correspond to the HOMO energies.

System	E_f (eV)	$E_f - E_f(0)$ (eV)	$E_f - E_f(II)$ (eV)	E_g (eV)
CO ₂	-10.7252	-	-	11.7521
CO ₂ *	-9.0689	-	-	8.6425
Imidazole	-6.1671	0	-	7.7999
Imidazole*	-5.0463	0	-	5.4592
Imidazole-CO ₂ (Im-CO ₂ I)	-6.4060	-0.2389	-	7.7918
Imidazole-CO ₂ (Im-CO ₂ I)*	-5.3156	-0.2693	-	5.4451
Imidazole-CO ₂ (Im-CO ₂ II)	-6.4921	-0.3250	-	7.6702
Imidazole-CO ₂ (Im-CO ₂ II)*	-5.4012	-0.3549	-	5.2447
Imidazole-CO ₂ (Im-CO ₂ III)	-6.0058	0.1613	-	6.3921
Imidazole-CO ₂ (Im-CO ₂ III)*	-4.8891	0.1572	-	3.8381
Graphene	-3.4697	0	-	0
Graphene*	-3.3652	0	-	0
Graphene-CO ₂ (G-I)	-3.5321	-0.0624	-	0
Graphene-CO ₂ (G-I)*	-3.4326	-0.0674	-	0
Graphene-imidazole (G-II)	-3.5976	-0.1279	0	0
Graphene-imidazole (G-II)*	-3.5007	-0.1355	0	0
Graphene-imidazole-CO ₂ (G-III)	-3.6311	-0.1614	-0.0335	0
Graphene-imidazole-CO ₂ (G-III)*	-3.5367	-0.1716	-0.0361	0
Graphene-imidazole-CO ₂ (G-IV)	-3.6768	-0.2072	-0.0792	0
Graphene-imidazole-CO ₂ (G-IV)*	-3.5892	-0.2240	-0.0885	0
Graphene-imidazole-CO ₂ (G-V)	-3.5944	-0.1247	0.0032	0
Graphene-imidazole-CO ₂ (G-V)*	-3.4972	-0.1320	0.0035	0
SWNT(5,5) (55-0)*	-3.3141	0	-	0
SWNT(5,5)-CO ₂ (55-I)*	-3.3580	-0.0440	-	0
SWNT(5,5)-imidazole (55-II)*	-3.3519	-0.0378	0	0
SWNT(5,5)-imidazole-CO ₂ (55-III)*	-3.4038	-0.0897	-0.0519	0
SWNT(8,0) (80-0)	-4.2250	0	-	1.5716
SWNT(8,0)-CO ₂ (80-I)	-4.2865	-0.0615	-	1.5728
SWNT(8,0)-imidazole (80-II)	-4.2754	-0.0504	0	1.5619
SWNT(8,0)-imidazole-CO ₂ (80-III)	-4.2982	-0.0733	-0.0228	1.5621

*PBE-D3/pob-TZVP

The analysis of charge repartitions in G-III, G-IV, and G-V from Table 5 values confirms that the graphene is p-doped, in agreement with the Fermi level variations. The charge variations from the situation where CO₂ is added to the graphene-imidazole system can be understood differently depending on the interaction geometries between imidazole and CO₂. For G-III and G-V, the imidazole and CO₂ molecules are approximately in the same plane and both interact with graphene in such a way that both can attract electrons from graphene. Only weak electron transfers exist between the adsorbed imidazole and CO₂. In the G-IV complex, the geometry (see Figure 2) is such that CO₂ interacts mainly with imidazole, and the final charge on CO₂ is almost identical to the CO₂ charge in Im-CO₂ II. This result is coherent with the weaker binding energy of CO₂ with graphene-imidazole in G-IV. Then, the graphene charge is almost invariant to the CO₂ adsorption in G-IV unlike G-III and G-V for which the positive charge in graphene is increased by ~0.6 e by the CO₂ presence (see Table 5).

Table 5. The net charge (Δq) from Mulliken analysis at the PBE0-D3/pob-TZVP and *PBE-D3/pob-TZVP levels of theory. The geometrical structures are shown in Figure 2.

System	$\Delta q(A)$ (e)	$\Delta q(B)$ (e)	$\Delta q(C)$ (e)
Imidazole-CO ₂ (Im-CO ₂ I)	0.02703	-0.02703	
Imidazole-CO ₂ (Im-CO ₂ I)*	0.03689	-0.03689	
Imidazole-CO ₂ (Im-CO ₂ II)	0.04901	-0.04901	
Imidazole-CO ₂ (Im-CO ₂ II)*	0.05526	-0.05526	
Imidazole-CO ₂ (Im-CO ₂ III)	-0.00463	0.00463	
Imidazole-CO ₂ (Im-CO ₂ III)*	-0.00537	0.00537	
Graphene-CO ₂ (G-I)	0.08377	-0.08377	
Graphene-CO ₂ (G-I)*	0.08784	-0.08784	
Graphene-imidazole (G-II)	0.08485	-0.08485	
Graphene-imidazole (G-II)*	0.08952	-0.08952	
Graphene-imidazole-CO ₂ (G-III)	0.14526	-0.05592	-0.08934
Graphene-imidazole-CO ₂ (G-III)*	0.15167	-0.05260	-0.09907
Graphene-imidazole-CO ₂ (G-IV)	0.09170	-0.04019	-0.05151
Graphene-imidazole-CO ₂ (G-IV)*	0.09695	-0.03824	-0.05870
Graphene-imidazole-CO ₂ (G-V)	0.15138	-0.07817	-0.07322
Graphene-imidazole-CO ₂ (G-V)*	0.15700	-0.07944	-0.07756
SWNT(5,5)-CO ₂ (55-I)*	0.08428	-0.08428	
SWNT(5,5)-imidazole (55-II)*	0.05139	-0.05139	
SWNT(5,5)-imidazole-CO ₂ (55-III)*	0.06063	-0.00361	-0.05703
SWNT(8,0)-CO ₂ (80-I)	0.07669	-0.07669	
SWNT(8,0)-imidazole (80-II)	0.06069	-0.06069	
SWNT(8,0)-imidazole-CO ₂ (80-III)	0.10525	-0.03125	-0.07400

*PBE-D3BJ/pob-TZVP

For SWNT including systems, the variations of the Fermi levels with the imidazole adsorption followed by the CO₂ capture, are in agreement with the charge transfers. For both SWNTs, the adsorption of CO₂ after functionalization of the SWNTs by imidazole provokes a weak increase of the amount of the positive charge on the SWNT and a lowering of the Fermi level. The positive charge is larger in SWNT(8,0) than in SWNT(5,5) for the same geometrical reasons than in graphene systems. The Fermi level lowering also follows the HOMO variations of imidazole subject to the different CO₂ adsorption geometries.

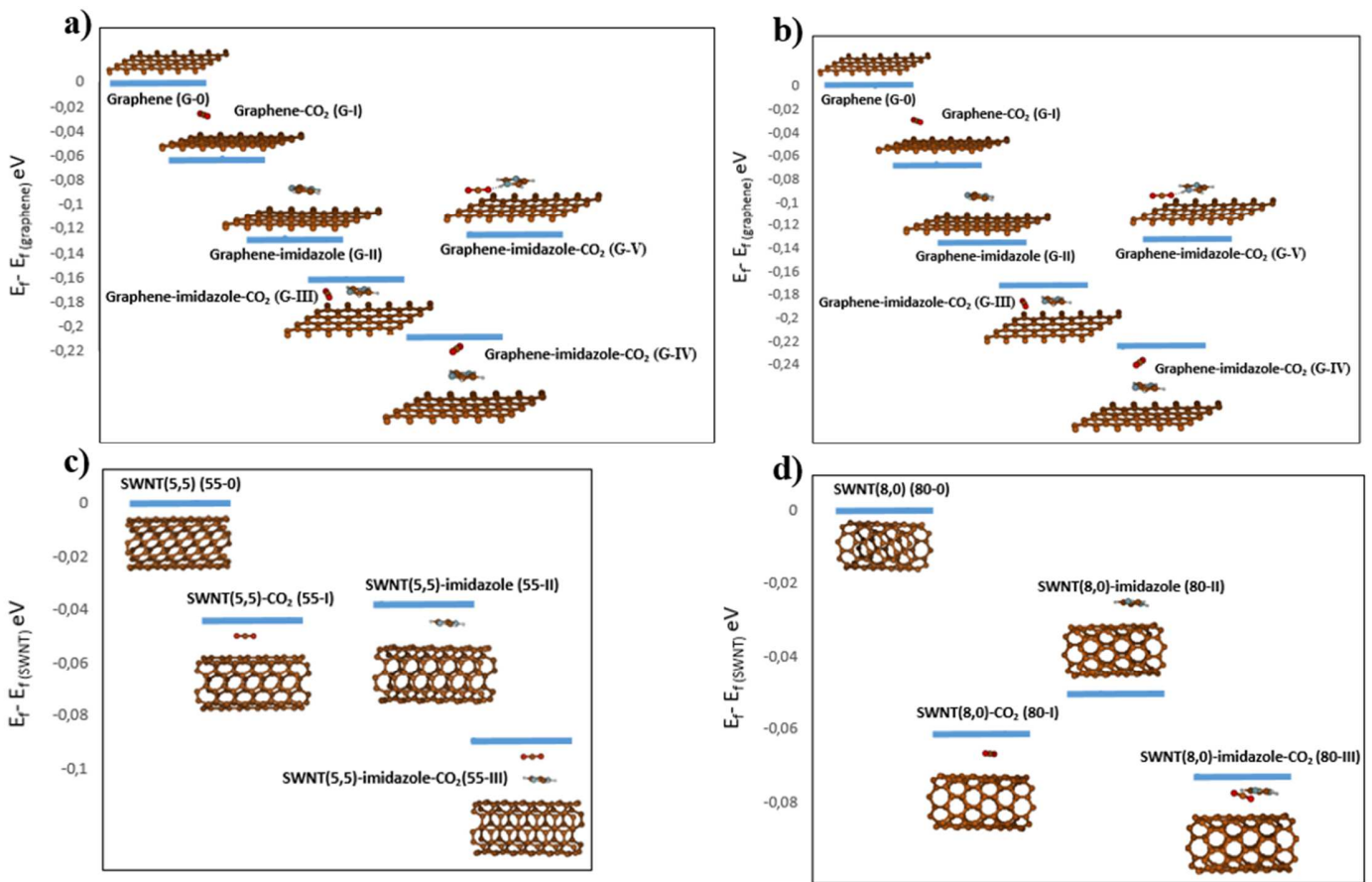


Figure 3. The variation of Fermi levels for: a) Graphene, graphene-CO₂, graphene-imidazole and graphene-imidazole-CO₂ at the PBE0-D3BJ/pob-TZVP level. b) Graphene, graphene-CO₂, graphene-imidazole and graphene-imidazole-CO₂ at the PBE-D3BJ/pob-TZVP level. c) SWNT(5,5), SWNT(5,5)-CO₂, SWNT(5,5)-imidazole and SWNT(5,5)-imidazole-CO₂ at the PBE-D3BJ/pob-TZVP level, d) SWNT(8,0), SWNT(8,0)-CO₂, SWNT(8,0)-imidazole and SWNT(8,0)-imidazole-CO₂ at the PBE0-D3BJ/pob-TZVP level.

For completeness of the present study, the total density of states (DOS) of graphene, graphene-CO₂, graphene-imidazole and graphene-imidazole-CO₂ for configurations (G-III), (G-IV) and (G-

V) using PBE and PBE0 are presented in Figures 4, SI 1, and SI 2 of the Supplementary Information, respectively. For the SWNT(5,5)/SWNT(8,0), SWNT(5,5)-CO₂/SWNT(8,0)-CO₂, SWNT(5,5)-imidazole/SWNT(8,0)-imidazole and SWNT(5,5)-midazole-CO₂/SWNT(8,0)-midazole-CO₂ the total DOS are shown in Figure 5. In order to highlight the contribution of each constituent of the complexes, the molecular orbitals of the molecular fragments (imidazole and CO₂) computed at the equilibrium geometries have also been shown.

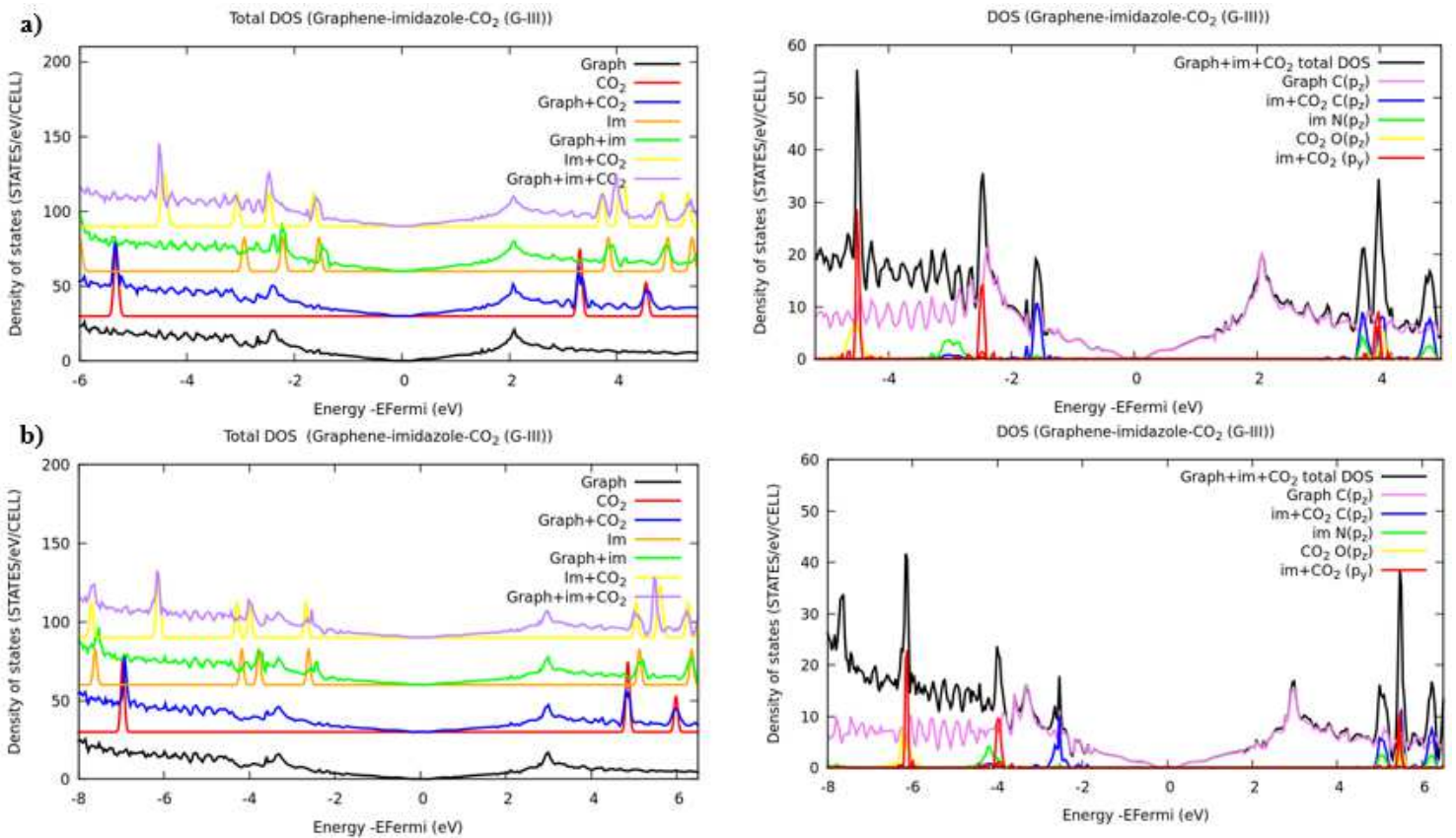


Figure 4. Densities of states, DOS, of graphene, graphene-CO₂, graphene-imidazole and graphene-imidazole-CO₂, (G-III structure), a) at PBE-D3BJ/pob-TZVP level, b) at PBE0-D3BJ/pob-TZVP level. In each figure, the Fermi level has been centered on 0. Projections of DOS for C p_z from graphene, C, N and O (p_z and p_y orbitals) from imidazole+CO₂ are displayed in purple, blue, green, yellow and red.

To allow easily assign the present molecular orbitals in the DOS of the material, a shift (work function) of the global molecular energy spectrum towards the DOS of the extended system was applied. The Dirac points of graphene systems have been chosen as energy reference. The DOS estimate of the gap is 0 eV for SWNT(5,5) and 1.56 eV for SWNT(8,0).

For each system, the total DOS is projected onto the atomic orbitals (PDOS) and the contributions of C ($2p_z/2p_y$) of graphene/SWNTs and C, N and O ($2p_z$ and $2p_y/2p_x$ orbitals) of imidazole- CO_2 are also plotted in Figures 4, 5, SI 1, and SI 2. The PBE0 DOS peaks are more separated than the PBE ones in agreement with the gap values obtained using both functionals (see Tables 1 and 4). In Figures 4 and 5, the adsorption of imidazole on graphene and on SWNTs causes apparition of new peaks in the DOS for energies lower than -1.5 eV and larger than 3 eV with PBE. The first peak around -1.5 eV with PBE corresponds to the HOMO of imidazole. The HOMO-1 orbital of imidazole (second peak towards the lower energies) corresponds to $2p_y$ orbitals for (G-III) and to $2p_z$ for (55-III) and (80-III). For symmetry reasons, these orbitals do not interact with any orbitals of the materials. The shifting the DOS peak related to O towards the Fermi level after the addition of CO_2 onto the graphene/SWNTs-imidazole complexes confirms the positive doping of functionalized materials.

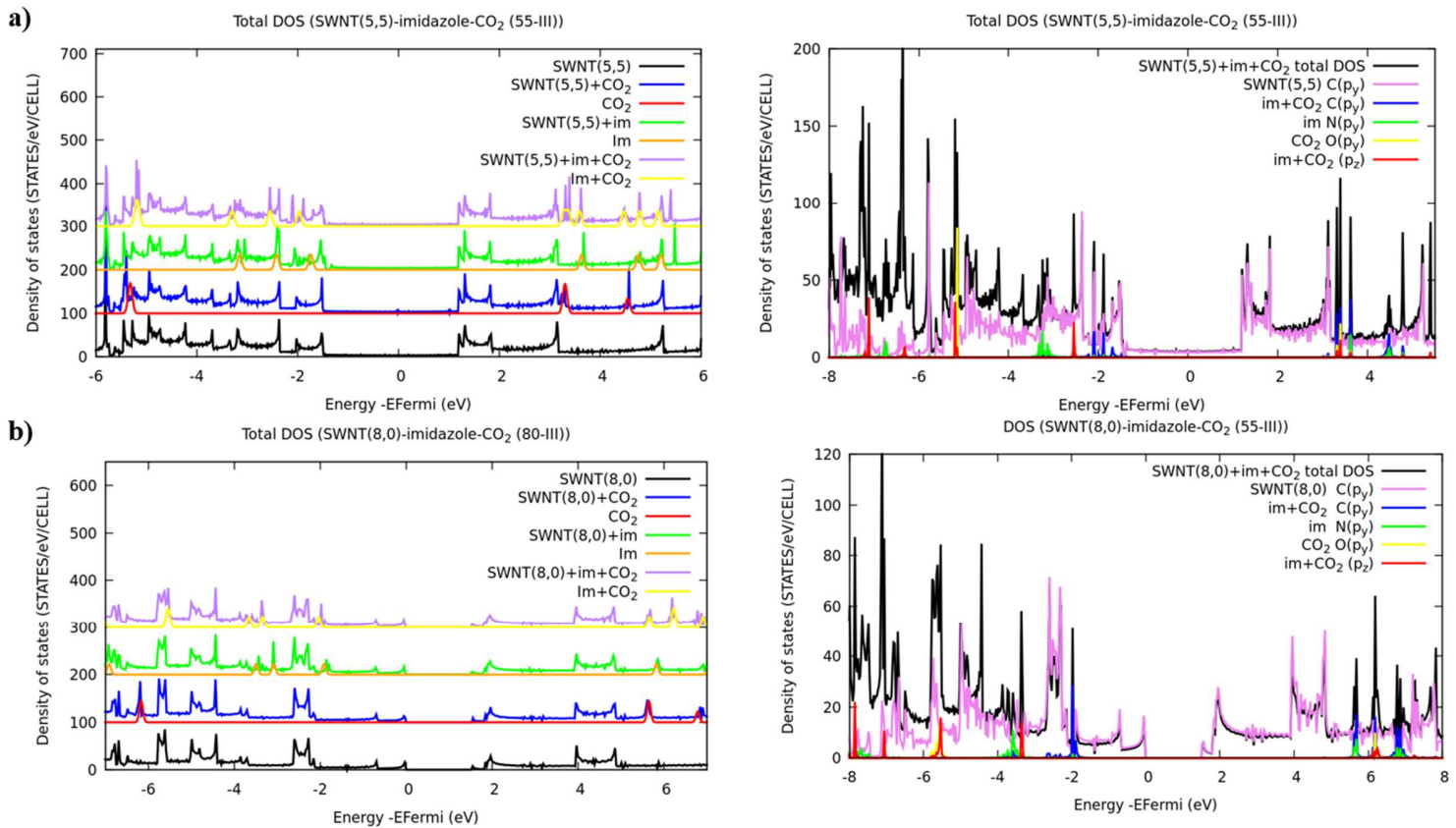


Figure 5. Densities of states, DOS, of a) SWNT(5,5), SWNT(5,5)- CO_2 , SWNT(5,5)-imidazole and SWNT(5,5)-imidazole- CO_2 at PBE-D3BJ/pob-TZVP level, b) SWNT(8,0), NTC(8,0)- CO_2 , NTC(8,0)-imidazole and NTC(8,0)-imidazole- CO_2 at PBE0-D3BJ/pob-TZVP level. In each figure, the Fermi level

has been centered on 0. Projections of DOS for C p_y from SWNTs, C, N and O (p_y and p_z orbitals) from imidazole+CO₂ are displayed in purple, blue, green, yellow and red.

4. Conclusions

The present study analyzes the effect of the adsorption of the CO₂ molecules on carbon nanomaterials functionalized by imidazole. These carbon nanomaterials-imidazole complexes have been chosen as simple prototypes of CO₂ sensors. The goal was to explore the effect of imidazole as functionalizing molecule on possible improvement of the CO₂ detection.

Three types of carbon nanomaterials have been studied: semi-metallic (graphene), metallic (SWNT(5,5)), and semi-conducting (SWNT(8,0)). For each case, the physisorption of CO₂, imidazole, and imidazole-CO₂ have been investigated by performing the geometry optimization of all the structures, and by computing electronic properties (bandgap energies, Fermi levels, Mulliken charges).

The main conclusions are: i) the results of the calculations with two different functionals PBE-D3 and PBE0-D3 are similar; ii) physisorption lead to a p-doping of carbon materials in all cases; iii) the presence of imidazole on graphene and semi-conducting SWNT(8,0) enforced the attachment of CO₂ and the creation of positive charges in the materials. This result confirms that the functionalization is an excellent strategy to improve the CO₂ detection with carbon nanomaterials.; iv) however, the interactions between the molecules and the carbon nanomaterials are weak (less than 40 kJ.mol⁻¹) and the influence on their electronic properties is then also weak, confirming that the non-covalent functionalization only slightly affects the electronic properties of the material.

Trends are observed and have been analyzed. Two different complex geometries have been found after the adsorption of CO₂ in functionalized nanomaterials. The first one is an in-plane conformation of imidazole-CO₂ interacting with the carbon material as in graphene-imidazole-CO₂ (G-III and G-V) and in SWNT(8,0)-imidazole-CO₂. These spatial organizations are associated with larger binding energies and larger positive charge on the functionalized material after CO₂ adsorption. The second one corresponds to a π -stacking type in graphene-imidazole-CO₂ (G-IV) and SWNTs(5,5)-imidazole-CO₂, with

weaker binding energies and almost no variation of the positive charge on the functionalized material after CO₂ adsorption. CO₂ attachment induces weak variations of the Fermi levels of graphene/SWNT-imidazole that follow those of the HOMO energies of the imidazole molecule. The Fermi level lowering after CO₂ adsorption is larger for π -stacking arrangements, i.e. in SWNT(5,5)-imidazole-CO₂ and in graphene-imidazole-CO₂ (G-IV).

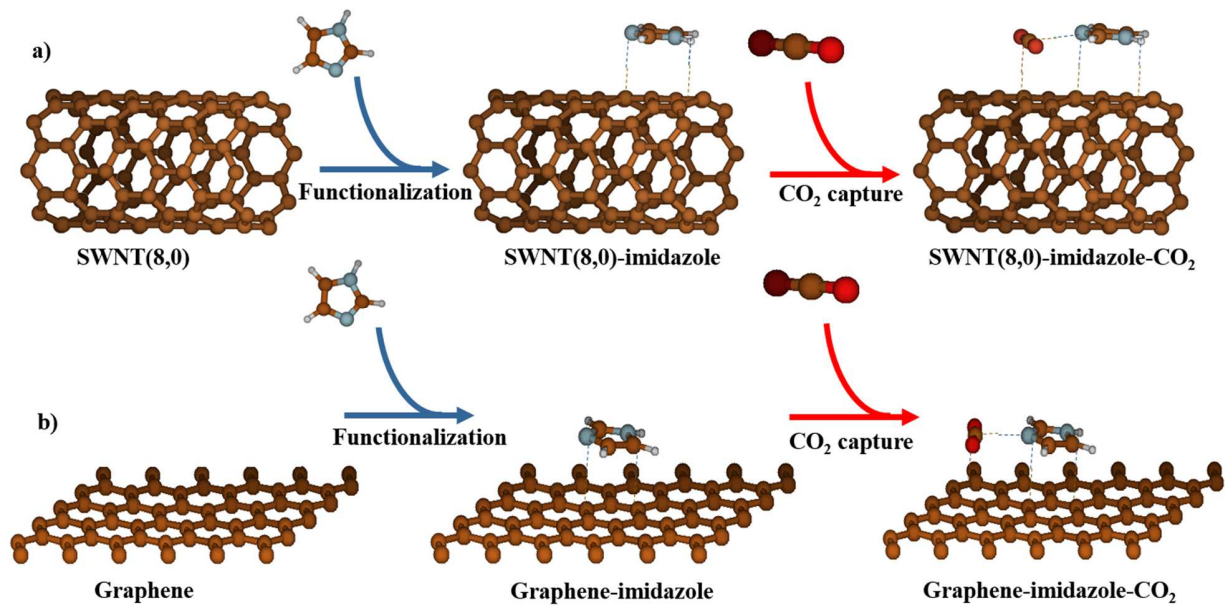


Figure 6. Schematic diagram of the functionalization of SWNT(8,0) a) and graphene b) by imidazole followed by the CO₂.

Finally, Figure 6 summarizes the different steps which allow the creation of larger positive charges on the functionalized carbon materials after the CO₂ capture. The most successful imidazole-functionalized materials for CO₂ detection are graphene and SWNT(8,0). The functionalization of semi-conducting nanotubes and graphene by imidazole leads more favorably to a π -type stacking geometry. This geometric organization allows the CO₂ molecule to favorably attach itself to the H-free nitrogen atom of imidazole. This fixing is accompanied by the creation of additional positive charges in the carbonated material.

5. Acknowledgments

The authors acknowledge financial support by the French National Research Agency under the Investissement d'Avenir program via COMUE UPE and Isite FUTURE (contract n° ANR-16-IDEX-0003). MB and CL would like to thank Dr Alexander MITRUSHCHENKOV for advices and fruitful discussions.

References

- (1) Liu, Z.; Guan, D.; Wei, W.; Davis, S. J.; Ciais, P.; Bai, J.; Peng, S.; Zhang, Q.; Hubacek, K.; Marland, G.; Andres, R. J.; Crawford-Brown, D.; Lin, J.; Zhao, H.; Hong, C.; Boden, T. A.; Feng, K.; Peters, G. P.; Xi, F.; Liu, J.; Li, Y.; Zhao, Y.; Zeng, N.; He, K. Reduced Carbon Emission Estimates from Fossil Fuel Combustion and Cement Production in China. *Nature* **2015**, *524* (7565). <https://doi.org/10.1038/nature14677>.
- (2) Jacobson, M. Z. Review of Solutions to Global Warming, Air Pollution, and Energy Security. *Energy and Environmental Science*. 2009. <https://doi.org/10.1039/b809990c>.
- (3) Liu, L.; Morgan, S. P.; Correia, R.; Lee, S. W.; Korposh, S. Multi-Parameter Optical Fiber Sensing of Gaseous Ammonia and Carbon Dioxide. *J. Light. Technol.* **2020**, *38* (7). <https://doi.org/10.1109/JLT.2019.2953271>.
- (4) Kuze, A.; Suto, H.; Nakajima, M.; Hamazaki, T. Thermal and near Infrared Sensor for Carbon Observation Fourier-Transform Spectrometer on the Greenhouse Gases Observing Satellite for Greenhouse Gases Monitoring. *Appl. Opt.* **2009**, *48* (35). <https://doi.org/10.1364/AO.48.006716>.
- (5) Imanaka, N.; Murata, T.; Kawasato, T.; Adachi, G. ya. CO₂ Detection with Lithium Solid Electrolyte Sensors. *Sensors Actuators B. Chem.* **1993**, *13* (1–3). [https://doi.org/10.1016/0925-4005\(93\)85431-9](https://doi.org/10.1016/0925-4005(93)85431-9).
- (6) Ratautaite, V.; Bagdziunas, G.; Ramanavicius, A.; Ramanaviciene, A. An Application of Conducting Polymer Polypyrrole for the Design of Electrochromic PH and CO₂ Sensors. *J. Electrochem. Soc.* **2019**, *166* (6). <https://doi.org/10.1149/2.1221904jes>.
- (7) Jamila, B.; Klumpp, A.; Hecker, C.; Eisele, I.; Yvonne, J. Functionalized Nanoparticles for CO₂ Sensor. *Funct. NANOSTRUCTURES Proc.* **2018**, 64–66.
- (8) Harris, P. J. F.; Hernández, E.; Yakobson, B. I. Carbon Nanotubes and Related Structures: New Materials for the Twenty-First Century. *Am. J. Phys.* **2004**, *72* (3). <https://doi.org/10.1119/1.1645289>.
- (9) Kong, J.; Franklin, N. R.; Zhou, C.; Chapline, M. G.; Peng, S.; Cho, K.; Dai, H. Nanotube Molecular Wires as Chemical Sensors. *Science (80-.)*. **2000**, *287* (5453). <https://doi.org/10.1126/science.287.5453.622>.
- (10) Li, D.; Kaner, R. B. Materials Science: Graphene-Based Materials. *Science*. 2008. <https://doi.org/10.1126/science.1158180>.
- (11) Dikin, D. A.; Stankovich, S.; Zimney, E. J.; Piner, R. D.; Dommett, G. H. B.; Evmenenko, G.; Nguyen, S. T.; Ruoff, R. S. Preparation and Characterization of Graphene Oxide Paper. *Nature* **2007**, *448* (7152). <https://doi.org/10.1038/nature06016>.
- (12) Saito, R.; Dresselhaus, G.; Dresselhaus, M. S. *Physical Properties of Carbon Nanotubes*; 1998. <https://doi.org/10.1142/p080>.
- (13) Geim, A. K.; Novoselov, K. S. The Rise of Graphene. *Nat. Mater.* **2007**, *6* (3). <https://doi.org/10.1038/nmat1849>.

- (14) Ge, L.; Mu, X.; Tian, G.; Huang, Q.; Ahmed, J.; Hu, Z. Current Applications of Gas Sensor Based on 2-D Nanomaterial: A Mini Review. *Frontiers in Chemistry*. 2019. <https://doi.org/10.3389/fchem.2019.00839>.
- (15) Bondavalli, P.; Legagneux, P.; Pribat, D. Carbon Nanotubes Based Transistors as Gas Sensors: State of the Art and Critical Review. *Sensors and Actuators, B: Chemical*. 2009. <https://doi.org/10.1016/j.snb.2009.04.025>.
- (16) Varghese, S. S.; Lonkar, S.; Singh, K. K.; Swaminathan, S.; Abdala, A. Recent Advances in Graphene Based Gas Sensors. *Sensors Actuators, B Chem*. **2015**, *218*. <https://doi.org/10.1016/j.snb.2015.04.062>.
- (17) Savagatrup, S.; Schroeder, V.; He, X.; Lin, S.; He, M.; Yassine, O.; Salama, K. N.; Zhang, X. X.; Swager, T. M. Bio-Inspired Carbon Monoxide Sensors with Voltage-Activated Sensitivity. *Angew. Chemie - Int. Ed*. **2017**, *56* (45). <https://doi.org/10.1002/anie.201707491>.
- (18) Qi, S.; Shuping, P.; Vajihah, A.; Chen, L.; Xinliang, F.; Müllen, K. Composites of Graphene with Large Aromatic Molecules. *Adv. Mater* **2009**, *21*, 3191–3195.
- (19) Xu, Y.; Bai, H.; Lu, G.; Li, C.; Shi, G. Flexible Graphene Films via the Filtration of Water-Soluble Noncovalent Functionalized Graphene Sheets. *J. Am. Chem. Soc*. **2008**, *130* (18). <https://doi.org/10.1021/ja800745y>.
- (20) Yang, H.; Shan, C.; Li, F.; Han, D.; Zhang, Q.; Niu, L. Covalent Functionalization of Polydisperse Chemically-Converted Graphene Sheets with Amine-Terminated Ionic Liquid. *Chem. Commun*. **2009**, No. 26. <https://doi.org/10.1039/b905085j>.
- (21) Ehli, C.; Aminur Rahman, G. M.; Jux, N.; Balbinot, D.; Guldi, D. M.; Paolucci, F.; Marcaccio, M.; Paolucci, D.; Melle-Franco, M.; Zerbetto, F.; Campidelli, S.; Prato, M. Interactions in Single Wall Carbon Nanotubes/Pyrene/Porphyrin Nanohybrids. *J. Am. Chem. Soc*. **2006**, *128* (34). <https://doi.org/10.1021/ja0624974>.
- (22) Magadur, G.; Lauret, J. S.; Charron, G.; Bouanis, F.; Norman, E.; Huc, V.; Cojocar, C. S.; Gómez-Coca, S.; Ruiz, E.; Mallah, T. Charge Transfer and Tunable Ambipolar Effect Induced by Assembly of Cu(II) Binuclear Complexes on Carbon Nanotube Field Effect Transistor Devices. *J. Am. Chem. Soc*. **2012**, *134* (18). <https://doi.org/10.1021/ja301362r>.
- (23) Georgakilas, V.; Otyepka, M.; Bourlinos, A. B.; Chandra, V.; Kim, N.; Kemp, K. C.; Hobza, P.; Zboril, R.; Kim, K. S. Functionalization of Graphene: Covalent and Non-Covalent Approaches, Derivatives and Applications. *Chemical Reviews*. 2012. <https://doi.org/10.1021/cr3000412>.
- (24) Kyatskaya, S.; Mascarós, J. R. G.; Bogani, L.; Hennrich, F.; Kappes, M.; Wernsdorfer, W.; Ruben, M. Anchoring of Rare-Earth-Based Single-Molecule Magnets on Single-Walled Carbon Nanotubes. *J. Am. Chem. Soc*. **2009**, *131* (42). <https://doi.org/10.1021/ja906165e>.
- (25) Zhao, Y. L.; Stoddart, J. F. Noncovalent Functionalization of Single-Walled Carbon Nanotubes. *Acc. Chem. Res*. **2009**, *42* (8). <https://doi.org/10.1021/ar900056z>.
- (26) Kumar, S.; Paveleyev, V.; Mishra, P.; Tripathi, N. Thin Film Chemiresistive Gas Sensor on Single-Walled Carbon Nanotubes-Functionalized with Polyethylenimine (PEI) for NO₂ Gas Sensing. *Bull. Mater. Sci*. **2020**, *43* (1). <https://doi.org/10.1007/s12034-020-2043-6>.

- (27) Zanolli, Z.; Leghrib, R.; Felten, A.; Pireaux, J. J.; Llobet, E.; Charlier, J. C. Gas Sensing with Au-Decorated Carbon Nanotubes. *ACS Nano* **2011**, *5* (6). <https://doi.org/10.1021/nn200294h>.
- (28) Bouanis, F. Z.; Bensifia, M.; Florea, I.; Mahouche-cherqui, S.; Carbonnier, B.; Grande, D.; Léonard, C.; Yassar, A.; Pribat, D. Non-Covalent Functionalization of Single Walled Carbon Nanotubes with Fe-/Co-Porphyrin and Co-Phthalocyanine for Field-Effect Transistor Applications. *Org. Electron.* **2021**, *96*. <https://doi.org/10.1016/j.orgel.2021.106212>.
- (29) Arramel; Castellanos-Gomez, A.; van Wees, B. J. Band Gap Opening of Graphene by Noncovalent π - π Interaction with Porphyrins. *Graphene* **2013**, *2013* (03), 102–108. <https://doi.org/10.4236/GRAPHENE.2013.23015>.
- (30) Bouanis, F.; Bensifia, M.; Florea, I.; Mahouche-Chergui, S.; Carbonnier, B.; Grande, D.; Léonard, C.; Yassar, A.; Pribat, D. Raw and Processed Data Used in Non-Covalent Functionalization of Single Walled Carbon Nanotubes with Co-Porphyrin and Co-Phthalocyanine and Its Effect on Field-Effect Transistor Characteristics. *Data Br.* **2021**, *38*. <https://doi.org/10.1016/j.dib.2021.107366>.
- (31) Zhou, Y.; Fang, Y.; Ramasamy, R. P. Non-Covalent Functionalization of Carbon Nanotubes for Electrochemical Biosensor Development. *Sensors (Switzerland)*. 2019. <https://doi.org/10.3390/s19020392>.
- (32) Dai, Y.; Ruan, X.; Yan, Z.; Yang, K.; Yu, M.; Li, H.; Zhao, W.; He, G. Imidazole Functionalized Graphene Oxide/PEBAX Mixed Matrix Membranes for Efficient CO₂ Capture. *Sep. Purif. Technol.* **2016**, *166*. <https://doi.org/10.1016/j.seppur.2016.04.038>.
- (33) Gevaerd, A.; Blaskievicz, S. F.; Zarbin, A. J. G.; Orth, E. S.; Bergamini, M. F.; Marcolino-Junior, L. H. Nonenzymatic Electrochemical Sensor Based on Imidazole-Functionalized Graphene Oxide for Progesterone Detection. *Biosens. Bioelectron.* **2018**, *112*. <https://doi.org/10.1016/j.bios.2018.04.044>.
- (34) Garg, N.; Kumar, M.; Kumari, N.; Deep, A.; Sharma, A. L. Chemoresistive Room-Temperature Sensing of Ammonia Using Zeolite Imidazole Framework and Reduced Graphene Oxide (ZIF-67/RGO) Composite. *ACS Omega* **2020**, *5* (42). <https://doi.org/10.1021/acsomega.0c03981>.
- (35) Demir-Cakan, R.; Makowski, P.; Antonietti, M.; Goettmann, F.; Titirici, M. M. Hydrothermal Synthesis of Imidazole Functionalized Carbon Spheres and Their Application in Catalysis. *Catal. Today* **2010**, *150* (1–2). <https://doi.org/10.1016/j.cattod.2009.05.003>.
- (36) Li, Y.; Li, G.; Wang, X.; Zhu, Z.; Ma, H.; Zhang, T.; Jin, J. Poly(Ionic Liquid)-Wrapped Single-Walled Carbon Nanotubes for Sub-Ppb Detection of CO₂. *Chem. Commun.* **2012**, *48* (66). <https://doi.org/10.1039/c2cc33365a>.
- (37) Dovesi, R.; Erba, A.; Orlando, R.; Zicovich-Wilson, C. M.; Civalieri, B.; Maschio, L.; Rérat, M.; Casassa, S.; Baima, J.; Salustro, S.; Kirtman, B. Quantum-Mechanical Condensed Matter Simulations with CRYSTAL. *Wiley Interdiscip. Rev. Comput. Mol. Sci.* **2018**, *8* (4). <https://doi.org/10.1002/wcms.1360>.
- (38) Adamo, C.; Barone, V. Toward Reliable Density Functional Methods without Adjustable Parameters: The PBE0 Model. *J. Chem. Phys.* **1999**, *110* (13). <https://doi.org/10.1063/1.478522>.
- (39) Paier, J.; Marsman, M.; Kresse, G. Why Does the B3LYP Hybrid Functional Fail for Metals? *J. Chem.*

- Phys.* **2007**, *127* (2). <https://doi.org/10.1063/1.2747249>.
- (40) Perdew, J. P.; Burke, K.; Ernzerhof, M. Generalized Gradient Approximation Made Simple. *Phys. Rev. Lett.* **1996**, *77* (18). <https://doi.org/10.1103/PhysRevLett.77.3865>.
- (41) Dai, J.; Yuan, J.; Giannozzi, P. Gas Adsorption on Graphene Doped with B, N, Al, and S: A Theoretical Study. *Appl. Phys. Lett.* **2009**, *95* (23). <https://doi.org/10.1063/1.3272008>.
- (42) Wu, X.; Zeng, X. C. Periodic Graphene Nanobuds. *Nano Lett.* **2009**, *9* (1). <https://doi.org/10.1021/nl802832m>.
- (43) Suggs, K.; Reuven, D.; Wang, X. Q. Electronic Properties of Cycloaddition-Functionalized Graphene. *J. Phys. Chem. C* **2011**, *115* (8). <https://doi.org/10.1021/jp111637b>.
- (44) Peintinger, M. F.; Oliveira, D. V.; Bredow, T. Consistent Gaussian Basis Sets of Triple-Zeta Valence with Polarization Quality for Solid-State Calculations. *J. Comput. Chem.* **2013**, *34* (6). <https://doi.org/10.1002/jcc.23153>.
- (45) Grimme, S.; Ehrlich, S.; Goerigk, L. Effect of the Damping Function in Dispersion Corrected Density Functional Theory. *J. Comput. Chem.* **2011**, *32* (7). <https://doi.org/10.1002/jcc.21759>.
- (46) Kratzer, P.; Neugebauer, J. The Basics of Electronic Structure Theory for Periodic Systems. *Frontiers in Chemistry*. 2019. <https://doi.org/10.3389/fchem.2019.00106>.
- (47) Dovesi, R.; Erba, A.; Orlando, R.; Zicovich-Wilson, C. M.; Civalieri, B.; Maschio, L.; Rerat, M.; Casassa, S.; Baima, J.; Salustro, S.; Kirtman, B. Crystal17. *WIREs Comput. Mol. Sci.* **2018**.
- (48) Mulliken, R. S. Electronic Population Analysis on LCAO-MO Molecular Wave Functions. I. *J. Chem. Phys.* **1955**, *23* (10). <https://doi.org/10.1063/1.1740588>.
- (49) Turi, L.; Dannenberg, J. J. Correcting for Basis Set Superposition Error in Aggregates Containing More than Two Molecules: Ambiguities in the Calculation of the Counterpoise Correction. *J. Phys. Chem.* **1993**, *97* (11). <https://doi.org/10.1021/j100113a002>.
- (50) Boys, S. F.; Bernardi, F. The Calculation of Small Molecular Interactions by the Differences of Separate Total Energies. Some Procedures with Reduced Errors. *Mol. Phys.* **1970**, *19* (4). <https://doi.org/10.1080/00268977000101561>.
- (51) Frisch, M. J.; Trucks, G. W.; Schlegel, H. E.; Scuseria, G. E.; Robb, M. A.; Cheeseman, J. R.; Scalmani, G.; Barone, V.; Petersson, G. A.; O., F.; Foresman, J. B.; Fox, J. D. Gaussian 16. *Gaussian, Inc., Wallingford CT*, 2016.
- (52) Lu, T.; Chen, F. Multiwfn: A Multifunctional Wavefunction Analyzer. *J. Comput. Chem.* **2012**, *33* (5). <https://doi.org/10.1002/jcc.22885>.
- (53) Slater, J. C. A Simplification of the Hartree-Fock Method. *Phys. Rev.* **1951**, *81* (3). <https://doi.org/10.1103/PhysRev.81.385>.
- (54) Cohen, A. J.; Mori-Sánchez, P.; Yang, W. Fractional Charge Perspective on the Band Gap in Density-Functional Theory. *Phys. Rev. B - Condens. Matter Mater. Phys.* **2008**, *77* (11). <https://doi.org/10.1103/PhysRevB.77.115123>.

- (55) Luna, C. R.; Verdinelli, V.; Germán, E.; Seitz, H.; Volpe, M. A.; Pistonesi, C.; Jasen, P. V. Hydrogen Adsorption and Associated Electronic and Magnetic Properties of Rh-Decorated (8,0) Carbon Nanotubes Using Density Functional Theory. *J. Phys. Chem. C* **2015**, *119* (23). <https://doi.org/10.1021/acs.jpcc.5b01407>.
- (56) Verdinelli, V.; Germán, E.; Luna, C. R.; Marchetti, J. M.; Volpe, M. A.; Juan, A. Theoretical Study of Hydrogen Adsorption on Ru-Decorated (8,0) Single-Walled Carbon Nanotube. *J. Phys. Chem. C* **2014**, *118* (48). <https://doi.org/10.1021/jp508183t>.
- (57) Liu, Y.; Zhang, Q.; Zhang, R.; Wang, B.; Hao, R.; Zhang, W.; Sang, S. Manipulating the Electronic Properties of CNT by Doping Metal. *Mater. Sci. Eng. B Solid-State Mater. Adv. Technol.* **2020**, *262*. <https://doi.org/10.1016/j.mseb.2020.114803>.
- (58) Matsuda, Y.; Tahir-Kheli, J.; Goddard, W. A. Definitive Band Gaps for Single-Wall Carbon Nanotubes. *J. Phys. Chem. Lett.* **2010**, *1* (19). <https://doi.org/10.1021/jz100889u>.
- (59) Weisman, R. B.; Bachilo, S. M. Dependence of Optical Transition Energies on Structure for Single-Walled Carbon Nanotubes in Aqueous Suspension: An Empirical Kataura Plot. *Nano Lett.* **2003**, *3* (9). <https://doi.org/10.1021/nl034428i>.
- (60) Bachilo, S. M.; Strano, M. S.; Kittrell, C.; Hauge, R. H.; Smalley, R. E.; Weisman, R. B. Structure-Assigned Optical Spectra of Single-Walled Carbon Nanotubes. *Science (80-.)*. **2002**, *298* (5602). <https://doi.org/10.1126/science.1078727>.
- (61) Baskin, Y.; Meyer, L. Lattice Constants of Graphite at Low Temperatures. *Phys. Rev.* **1955**, *100* (2). <https://doi.org/10.1103/PhysRev.100.544>.
- (62) Demichelis, R.; Noël, Y.; Darco, P.; Rérat, M.; Zicovich-Wilson, C. M.; Dovesi, R. Properties of Carbon Nanotubes: An Ab Initio Study Using Large Gaussian Basis Sets and Various DFT Functionals. *J. Phys. Chem. C* **2011**, *115* (18). <https://doi.org/10.1021/jp110704x>.
- (63) Sun, G.; Kürti, J.; Kertesz, M.; Baughman, R. H. Variations of the Geometries and Band Gaps of Single-Walled Carbon Nanotubes and the Effect of Charge Injection. *J. Phys. Chem. B* **2003**, *107* (29). <https://doi.org/10.1021/jp022629p>.
- (64) Umari, P.; Petrenko, O.; Taioli, S.; De Souza, M. M. Communication: Electronic Band Gaps of Semiconducting Zig-Zag Carbon Nanotubes from Many-Body Perturbation Theory Calculations. *J. Chem. Phys.* **2012**, *136* (18). <https://doi.org/10.1063/1.4716178>.
- (65) Spataru, C. D.; Ismail-Beigi, S.; Benedict, L. X.; Louie, S. G. Excitonic Effects and Optical Spectra of Single-Walled Carbon Nanotubes. *Phys. Rev. Lett.* **2004**, *92* (7). <https://doi.org/10.1103/PhysRevLett.92.077402>.
- (66) Kang, W.; Hybertsen, M. S. Enhanced Static Approximation to the Electron Self-Energy Operator for Efficient Calculation of Quasiparticle Energies. *Phys. Rev. B - Condens. Matter Mater. Phys.* **2010**, *82* (19). <https://doi.org/10.1103/PhysRevB.82.195108>.
- (67) Maultzsch, J.; Telg, H.; Reich, S.; Thomsen, C. Radial Breathing Mode of Single-Walled Carbon Nanotubes: Optical Transition Energies and Chiral-Index Assignment. *Phys. Rev. B - Condens. Matter Mater. Phys.* **2005**, *72* (20). <https://doi.org/10.1103/PhysRevB.72.205438>.

- (68) Dalbouha, S.; Prakash, M.; Timón, V.; Komiha, N.; Hochlaf, M.; Senent, M. L. Explicitly Correlated Interaction Potential Energy Profile of Imidazole + CO₂ Complex. *Theor. Chem. Acc.* **2015**, *134* (5). <https://doi.org/10.1007/s00214-015-1657-z>.
- (69) Prakash, M.; Mathivon, K.; Benoit, D. M.; Chambaud, G.; Hochlaf, M. Carbon Dioxide Interaction with Isolated Imidazole or Attached on Gold Clusters and Surface: Competition between σ H-Bond and π Stacking Interaction. *Phys. Chem. Chem. Phys.* **2014**, *16* (24). <https://doi.org/10.1039/c4cp01292e>.
- (70) De Lara-Castells, M. P.; Bartolomei, M.; Mitrushchenkov, A. O.; Stoll, H. Transferability and Accuracy by Combining Dispersionless Density Functional and Incremental Post-Hartree-Fock Theories: Noble Gases Adsorption on Coronene/Graphene/Graphite Surfaces. *J. Chem. Phys.* **2015**, *143* (19). <https://doi.org/10.1063/1.4935511>.
- (71) Cabrera-Sanfeliu, P. Adsorption and Reactivity of CO₂ on Defective Graphene Sheets. *J. Phys. Chem. A* **2009**, *113* (2). <https://doi.org/10.1021/jp807087y>.
- (72) Takeuchi, K.; Yamamoto, S.; Hamamoto, Y.; Shiozawa, Y.; Tashima, K.; Fukidome, H.; Koitaya, T.; Mukai, K.; Yoshimoto, S.; Suemitsu, M.; Morikawa, Y.; Yoshinobu, J.; Matsuda, I. Adsorption of CO₂ on Graphene: A Combined TPD, XPS, and VdW-DF Study. *J. Phys. Chem. C* **2017**, *121* (5). <https://doi.org/10.1021/acs.jpcc.6b11373>.
- (73) Zhao, J.; Buldum, A.; Han, J.; Lu, J. P. Gas Molecule Adsorption in Carbon Nanotubes and Nanotube Bundles. *Nanotechnology* **2002**, *13* (2). <https://doi.org/10.1088/0957-4484/13/2/312>.
- (74) Nistor, R. A.; Newns, D. M.; Martyna, G. J. The Role of Chemistry in Graphene Doping for Carbon-Based Electronics. *ACS Nano* **2011**, *5* (4). <https://doi.org/10.1021/nn200225f>.
- (75) del Castillo, R. M.; Calles, A. G.; Espejel-Morales, R.; Hernández-Coronado, H. Adsorption of CO₂ on Graphene Surface Modified with Defects. *Comput. Condens. Matter* **2018**, *16*. <https://doi.org/10.1016/j.cocom.2018.e00315>.